Available online at www.sciencedirect.com

ScienceDirect

Nuclear Physics A 977 (2018) 112–128

NUCLEAR PHYSICS A

www.elsevier.com/locate/nuclphysa

Measurements and uncertainty propagation for the $^{nat}Ni(p, x)^{61}Cu$ reaction cross section up to the proton energies of 20 MeV

Sylvia Badwar [a], Reetuparna Ghosh [a], Santhi Sheela Yerraguntla [b], Betylda Mary Jyrwa [a], Bioletty Mary Lawriniang [a], Haladhara Naik [c], Yeshwant Naik [d], Saraswatula Venkata Suryanarayana [e], Srinivasan Ganesan [f]

[a] *Physics Department, North Eastern Hill University, Shillong-793022, Meghalaya, India*
[b] *Department of Statistics, M.A.H.E., Manipal, Karnataka-576104, India*
[c] *Radiochemistry Division, Bhabha Atomic Research Centre, Trombay, Mumbai-400085, India*
[d] *Product Development Division, Bhabha Atomic Research Centre, Mumbai-400085, India*
[e] *Nuclear Physics Division, Bhabha Atomic Research Centre, Trombay, Mumbai-400085, India*
[f] *Raja Ramana Fellow of HBNI, Bhabha Atomic Research Centre, Mumbai-400085, India*

Received 14 April 2018; received in revised form 24 June 2018; accepted 25 June 2018
Available online 28 June 2018

Abstract

The $^{nat}Ni(p, x)^{61}Cu$ reaction cross sections relative to $^{nat}Cu(p, x)^{62}Zn$ monitor reaction with proton energies up to 20 MeV have been measured using the stack foil activation and off-line γ-ray spectrometric technique. The error analysis of the experimental data was done by using the concept of covariance analysis. The present experimental cross sections have been compared with TALYS-1.8 and the results obtained well predicted the present experimental cross sections at the proton energies of 7.25, 15.70 and 18.89 MeV. The results from TALYS calculation are also in agreement with the earlier measurements available in the literature between the proton energies of 3–15 MeV, which confirms the reliability of the database. The $^{nat}Ni(p, x)^{61}Cu$ reaction cross sections obtained in the present work have been further compared with the data from TENDL-2015 libraries. They are found to be in excellent agreement with TENDL-2015 at 7.25 and 15.70 MeV. The present results along with detailed covariance information, which takes into account various attributes influencing the uncertainties and also the correlation between them, emphasize their sig-

E-mail address: naikhbarc@yahoo.com (H. Naik).

https://doi.org/10.1016/j.nuclphysa.2018.06.006

nificance during evaluation process in the proton induced reactions of natural nickel for the production of medically relevant radioisotope, ^{61}Cu.

Keywords: ^{nat}Ni$(p, x)^{61}$Cu reaction; Cross-section; Stack foil activation technique; Off-line γ-ray spectrometry; Covariance analysis; TALYS-1.8; TENDL-2015

1. Introduction

Nickel is one of the most frequently used structural materials (alloys, anti-corrosion), and thus its activation reaction cross-sections data are important when used in nuclear and space equipment working under intensive radiation [1]. Nickel is an important material used in accelerator and nuclear technology. It is incorporated in stainless steel, present as surface coating and is proposed as beam dump for high power accelerators [2]. Silvery-white metallic Ni is lustrous and resistive to corrosion. The vast industrial applications of nickel (Ni) metal, its compound and even its alloys have been perceived due to its physical and chemical properties. Hence, Ni has been given priority over other materials in a recent IAEA Coordinated Research Project on Nuclear Data Libraries for Advance Systems–Fusion Devices (FENDL-3) [3]. Moreover, the activation reaction cross-section data of nickel isotopes are of interest for the design studies of accelerator driven sub-critical system (ADSs) [4], thin layer activation (TLA) analysis and so on. Nickel can also be used as a target material for the production of several radionuclides of Co, Cu, Cr, Mn and Ni leading to industrial and medical application. Among them, produced radionuclides such as ^{60,61,62,64}Cu and ^{55,56,57,58}Co have potential applications in medicine [1,5]. The radionuclides ^{60,61,62,64}Cu are promising nuclides for labelling radiopharmaceuticals for Positron Emission Tomography (PET). Given their high positron branching ratio, ^{60}Cu ($T_{1/2} = 23.7$ min, $I_{\beta+} = 93\%$) and ^{62}Cu ($T_{1/2} = 9.7$ min, $I_{\beta+} = 98\%$) can render high quality PET images. However, their applications are limited by their short half-lives to uptake times shorter than 1 h. ^{64}Cu is an intermediate half-life nuclide ($T_{1/2} = 12.7$ h, $I_{\beta+} = 17.6\%$, $I_{\beta-} = 38.50\%$), currently used for imaging and therapy. Despite its less than desirable image quality, it is one of the few PET tracers available to study processes with uptake longer than 4 h [6]. ^{61}Cu ($T_{1/2} = 3.339$ h, $I_{\beta+} = 61\%$) is another radionuclide of copper with potential utilization in nuclear medicine due to its nuclear properties, desirable half-life and ease for production [7–9]. It decays mainly via positron emission accompanied with dominant γ-rays of 282.96 keV (12.2%) and 656.01 keV (10.8%). The detection sensitivity of ^{61}Cu is more than three times that of ^{64}Cu, when β^+ scintiscanning is used [10–12]. The relatively longer half-life of ^{61}Cu compared to ^{60}Cu and ^{62}Cu reduces the decay loss of radioactivity during the processing, and allows imaging of slower biological processes with low accuracy due to relatively high β^+ emission ratio [13]. ^{61}Cu could yield higher quality images than with ^{64}Cu, due to the higher positron decay branching and the shorter half-life. Thus, it covers the gap between the other radionuclides of copper and eases the commercial distribution from a centralized facility. For the investigation of copper distribution in patients suffering Wilson's disease ^{61}Cu[$CuCl_2$] has been used as a PET tracer [12]. It is considered to be a suitable candidate for studies of slow kinetics of larger proteins, such as peptides and antibodies, or cells [14]. ^{61}Cu is of special interest because of its large number of production possibilities. Several charged particles induced reactions on nickel, copper and zinc targets have been measured to produce ^{61}Cu [2,5,7,9,15–17]. In majority of the cases relatively high produc-

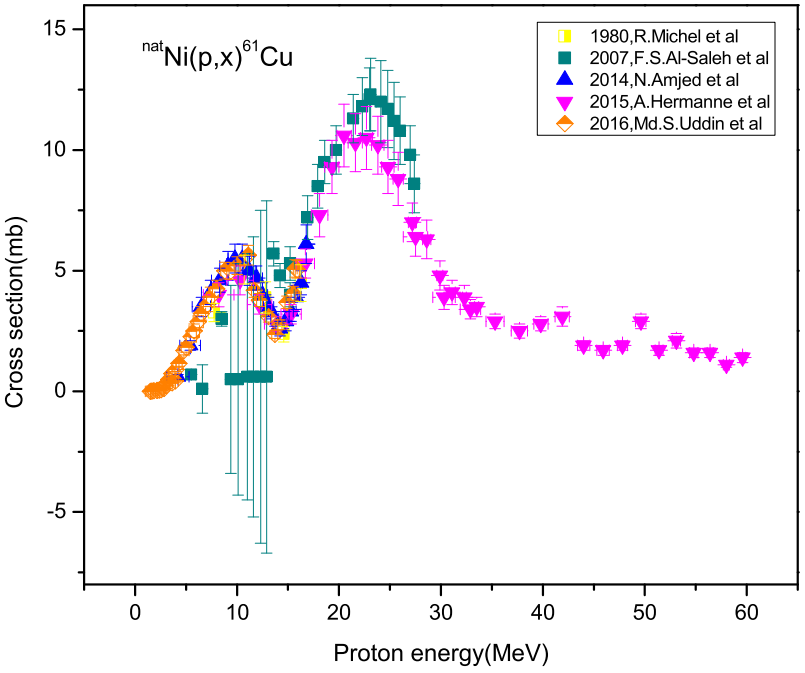

Fig. 1. Excitation function of the ^{nat}Ni$(p,x)^{61}$Cu reaction from EXFOR database.

tion yield of ^{61}Cu requires highly enriched target materials. The cost of the enriched targets, the necessity of the recovery of target materials after production and the material losses during the irradiation, separation and recovery steps are major disadvantages of these production ways. The ^{61}Ni$(p,n)^{61}$Cu reaction is one of the most important routes for the production of ^{61}Cu, but it needs very expensive highly enriched ^{61}Ni target material [7].

Literature survey on the experimental data [1,18–21] which are also available in IAEA-EXFOR database [22,23] shows the production of medically important radionuclide ^{61}Cu being carried out by proton bombardment on natural nickel targets. Fig. 1 shows that the agreement of literature data is generally good, except a single data set from Al-Saleh et al. [19], even if this data have poor quality between the proton energies around 8 and 13 MeV. The literature data [1,19–21] also indicate that the uncertainties associated with the existing ^{nat}Ni$(p,x)^{61}$Cu reaction cross sections were estimated by quadratic summation of the individual uncertainties contributing to the cross section, assuming they are independent. The interdependency between the uncertainties, if any, were either not observed or not reported. The data of R. Michel et al., [18] has no information on data uncertainties. These inconsistencies severely limit the reliability of data evaluations. Modern evaluation requires not only the best estimate of the reaction cross section but also the complete description of its uncertainty and covariance describing the correlation among them. Thus it is mandatory to provide covariance matrix that contains the essential information required for reliable estimation of the uncertainty [24]. New experimental data are therefore required, to improve the cross sections data in the database along with detail documentation of uncertainty propagation for evaluation process. In view of the above, the present work has been carried out for the measurement of ^{nat}Ni$(p,x)^{61}$Cu reaction cross sections within the proton energy range of 20 MeV down to the thresholds by using stack-foil activation technique and off-line gamma-ray spectrometry. The ^{nat}Ni$(p,x)^{61}$Cu reaction cross

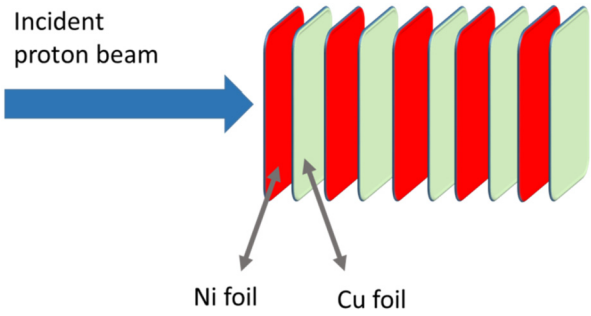

Fig. 2. Schematic diagram of the arrangement of the metal foils in stacked foil activation technique.

sections were measured relative to the $^{nat}Cu(p,x)^{62}Zn$ reaction cross sections. In the present work, the $^{nat}Cu(p,x)^{62}Zn$ monitor reaction was adopted as the reference cross-section and was taken from IAEA recommended charged-particle reference cross section library [1,25], which contains the recommended evaluated cross section of monitor reactions. The $^{nat}Cu(p,x)^{62}Zn$ monitor reaction was a preferable choice due to the activation product, ^{62}Zn, which has a relatively longer half-life ($T_{1/2} = 9.193$ h) than that of ^{63}Zn ($T_{1/2} = 38.47$ min) but it is shorter than that of ^{65}Zn ($T_{1/2} = 243.93$ d). This fact enables measurement of the monitor foils few hours after the end of irradiation. The error analysis of the experimental data was done by covariance analysis considering the partial uncertainties in various attributes and the correlations that exist between those attributes. The $^{nat}Ni(p,x)^{61}Cu$ reaction cross section as a function of proton energy was also calculated theoretically by using the computer code TALYS 1.8 [26] up to proton energy of 60 MeV with nuclear model parameters adjusted within their recommended limits to improve the agreement with experimental data.

2. Experimental procedures

2.1. Targets, stack formation and irradiation

The experiment for the measurement of $^{nat}Ni(p,x)^{61}Cu$ reaction cross section was performed by using the 14 UD BARC-TIFR Pelletron facility at Mumbai, India. The proton beam main line at 6 m above the analyzing magnet of the Pelletron facility was utilized to attain the maximum proton current from the accelerator. At this port, the terminal voltage was regulated by generating voltage mode (GVM) using a terminal potential stabilizer. The conventional stack-foil irradiation technique was carried out as done by most of the authors [1,18–21]. Nickel foils (99.99% purity; 101 μm thickness) having the natural isotopic composition (^{58}Ni, 68.077%; ^{60}Ni, 26.223%; ^{61}Ni, 1.140%; ^{62}Ni, 3.635%; ^{64}Ni, 0.926%) [27] were used as the target material. Similarly, natural copper foils (99.99% purity; 99.5 μm thickness) having natural isotopic abundance (^{63}Cu, 69.15%, ^{65}Cu, 30.85%) were also included in the stacks serving as the energy degrader along the stack and as a monitor. The stack-foil consisting of five identical pairs (Ni–Cu) metal foils was made by keeping the Ni and Cu foils alternately arranged in the order Ni–Cu–Ni–Cu–Ni–Cu–Ni–Cu–Ni–Cu. A schematic arrangement of the stack is shown in Fig. 2. The stack was additionally wrapped with 25 μm thick Al foil and then mounted at zero degree with respect to the beam direction. The monitor and target foils were prepared with a size of 8×8 mm^2 and the proton beam was collimated to 6 mm diameter to ensure that equal areas of the monitors and the target materials received the same beam flux during the experiment. The stack was irradiated

for 10 minutes with an initial proton beam of 20 MeV and the beam current of 100 nA was kept constant during the irradiation process. The energy of the incident proton beam decreases, as it passes through the stack and so the successive foils of the stack were irradiated with incident particles of different energies.

2.2. Gamma ray spectrometry of activation products

After the irradiation, the activated foils were sufficiently cooled and then mounted separately on the Perspex plates and taken for off-line γ-ray spectrometry. The emitted γ-rays from the activated target foils of the sample and monitor were measured non-destructively using a pre-calibrated lead shielded coaxial high-purity germanium (HPGe) detector with 51.3 mm crystal diameter and 58.7 mm crystal length having 20% relative efficiency. The energy resolution of the detector was 1.8 keV full width half maximum (FWHM) at the 1332.5 keV γ-ray photo-peak of ^{60}Co. The HPGe detector was coupled to a PC based 4k channel analyzer. The energy and efficiency calibration of the HPGe detector system was carried out by using a standard ^{152}Eu point source ($T_{1/2} = 13.517$ years) from its characteristic γ-ray energies [28] retrieved through NuDat 2.7β database [29]. The source detector system was maintained at a distance of 12 cm from the end cap of the detector to minimize pile up effect, to have low dead time ($<10\%$) and to suppress the sum-coincidence effect caused by the coincidental detection of two or more γ-rays emitted in cascade. Similarly, the measurements of the activated sample and monitor foils were counted one at a time. The irradiated targets in the present experiments have finite dimension thus, the efficiency obtained for the point source geometry was transferred to the dimensions of the samples geometry of finite size using code EFFTRAN [30]. The inputs for the simulation requires the specifications of the HPGe detector (e.g., dimension and crystal material, crystal hole cavity, window, end cap, mount cup and absorber), the ^{152}Eu γ-ray source (e.g. source dimension, characteristic γ-rays and x-rays) and the target samples dimensions.

3. Data analysis

3.1. Estimation of the efficiency of the HPGe detector along with the uncertainty propagation in efficiency calculation

The energy and efficiency calibration of the HPGe detector system was carried out by considering five γ-lines of the standard ^{152}Eu point source reported in Table 1. The source activity (A_0) was 7767.73 Bq on 1st October, 1999. The efficiency of detector was determined from the following equation

$$\varepsilon_p = \frac{C}{A_0 e^{-\lambda t} I_\gamma \Delta T} \tag{1}$$

where, C is the detected counts under the photo-peak of each γ-line during the counting time ΔT, λ ($= \ln 2/T_{1/2}$) is the decay constant for ^{152}Eu, t is the cooling time, i.e. the time elapsed between the date of manufacture to the start of counting time. I_γ is the branching intensity or abundance of γ-ray. The efficiency calibration of the HPGe detector was obtained for a point source ε_p, using Eq. (1) and is presented in Table 1. The efficiency transferred to the full-energy peak efficiency for the samples of finite size using EFFTRAN, ε is also presented in Table 1.

The sources of uncertainty associated with the different attributes (C, A_0, I_γ, $T_{1/2}$) in the calibration process was propagated into the uncertainty of the detector efficiency. All the above four

Table 1
Detection efficiencies for the point source geometry and sample geometry at the characteristic γ-ray energies of ^{152}Eu with corresponding γ-ray intensities [28,29].

Gamma-ray energy (keV)	Gamma-ray energy (MeV)	Gamma-ray intensity (%)	ε_p (efficiency for point source)	ε (efficiency of sample)
121.78	0.1218	28.53 ± 0.16	2.47E−03	2.37E−03
344.28	0.3443	26.59 ± 0.2	9.55E−04	9.17E−04
778.90	0.7789	12.93 ± 0.08	4.21E−04	4.05E−04
1112.08	1.1121	13.67 ± 0.08	2.60E−04	2.50E−04
1408.01	1.4080	20.87 ± 0.09	2.52E−04	2.42E−04

attributes are observed independently and the terms t and ΔT are determined without uncertainty and may be treated as constants, hence we can treat ε as function of variables C, A_0, I_γ and $T_{1/2}$ and the uncertainty propagation in efficiency of the HPGe detector was carried out following the methodology of L.P. Geraldo and D.L. Smith [31] as described in details in earlier measurements reported by Y. Santhi Sheela et al. [32] and R. Ghosh et al. [33,34]. The uncertainty in the efficiency (ε_i) due to the ith γ-line can be propagated as

$$(\Delta\varepsilon_i)^2 = \sum_k \left(\frac{\partial\varepsilon_i}{\partial x_{ki}}\Delta x_{ki}\right)^2, \quad 1 \le i \le 5,\ 1 \le k \le 4 \tag{2}$$

Similarly, the uncertainty in the efficiency (ε_j) due to the jth γ-line can be propagated as

$$(\Delta\varepsilon_j)^2 = \sum_k \left(\frac{\partial\varepsilon_j}{\partial x_{kj}}\Delta x_{kj}\right)^2, \quad 1 \le j \le 5,\ 1 \le k \le 4 \tag{3}$$

where x_k represents the attributes C, A_0, I_γ and $T_{1/2}$. The information on the partial errors due to each attributes and their correlations provides a basis for constructing the covariance matrix V_ε which completely represents the uncertainties in the measured efficiencies. Thus the elements of the covariance matrix (V_ε) due to the ith and jth γ-line is calculated as

$$V_{\varepsilon ij} = \sum_k \left(\frac{\partial\varepsilon_i}{\partial x_{ki}}\Delta x_{ki}\right) cor(x_{ki}, x_{kj}) \left(\frac{\partial\varepsilon_j}{\partial x_{kj}}\Delta x_{kj}\right), \quad 1 \le i, j \le 5,\ 1 \le k \le 4 \tag{4}$$

where $cor(x_{ki}, x_{kj})$ represents the micro correlation between ith γ-line and jth γ-line of the kth attribute. The micro correlation matrix corresponding to the attributes C and I_γ is an identity matrix I of order 5 as the observations were made independently. However, the micro correlation matrix in case of the attributes A_0 and $T_{1/2}$ is a matrix J with all entries equal to 1 and order 5 because the same decay constant and same source strength of ^{152}Eu was adopted in the efficiency calculation.

The characteristic γ-ray energies of the radionuclides of interest are different from the characteristic γ-ray energies of ^{152}Eu used in the calibration process hence in order to get the efficiencies at the 282.96 and 596.56 keV γ-lines of ^{61}Cu and ^{62}Zn, an appropriate model for interpolation was chosen using the following linear parametric function

$$\ln\varepsilon_i = \sum_n p_n (\ln E_i)^{n-1} \tag{5}$$

and the corresponding linear model as $Z \approx AP$ in matrix form, where $Z = \ln(\varepsilon_i)$, ε_i is the efficiency of the detector obtained at γ-ray energies E_i, A is the design matrix with elements

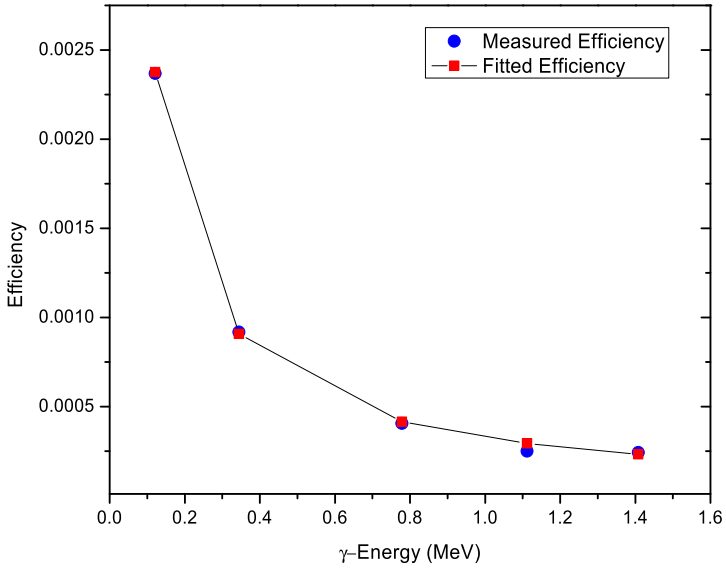

Fig. 3. The measured and fitted detection efficiency calibration curve of the HPGe detector calibrated at a distance of 12 cm from detector end cap window.

Table 2
Detector efficiencies of the reaction products with their uncertainties and corresponding correlation matrix.

Nuclide	γ-Ray energy (keV)	Efficiency ($\varepsilon \times 10^3$)	Correlation matrix
^{61}Cu	282.96	1.09 ± 0.05	1.00
^{62}Zn	596.56	0.54 ± 0.02	0.86
			1.00

$A_{i,n} = (\ln E_i)^{n-1}$ $(1 \leq n \leq m;\ 1 \leq i \leq 5)$ and P is a column matrix having elements p_n, which are unknown parameters to be estimated. The parameter n is varied to achieve the best model for interpolation and the selection was based on minimum Chi-square (χ^2) statistics [31–34]. We prefer to choose the model with $\chi^2/(i-n)$ closest to one. In the present work, the best fit was obtained for $n = 3$ with $\chi^2/(5-3) = 0.99 \approx 1$ and we consider the corresponding linear parametric model as the best model, which is given by

$$\ln \varepsilon_i = -8.03 - 0.98(\ln E_i) - 0.02(\ln E_i)^2 \tag{6}$$

The fitted efficiencies thus obtained for $n = 3$ model along with the measured efficiencies are shown in Fig. 3. The required efficiencies for the 282.96 and 596.56 keV γ-lines of ^{61}Cu and ^{62}Zn, along with their correlation are presented in Table 2.

3.2. Determination of cross section

The proton beam energy degradation along the stack can be calculated using the computer code SRIM 2013 of Ziegler [35] and a new method developed by Fisichella et al. [36], which were followed in the present work. As the stack containing the targets and monitor foils were

additionally wrapped with Al foil of 25 μm thick hence the proton energy loss in the Al foil was also considered. This is because the beam energy distribution degrades as it traverses through the stack [36]. Based on the SRIM [35] calculation, the average proton beam energy ($\langle E \rangle$) incident on the first Ni target was found to be 18.89 ± 0.76 MeV. For the other three Ni foils, the average proton beam energies are 15.70 ± 0.86, 11.97 ± 1.03 and 7.25 ± 1.39 MeV, respectively. The average proton energies are based on the mean energy of the beam particles entering the target (E_{in}) and the mean energy of the beam particles after completely traversing the target (E_{out}). In SRIM [35], E_{out} is usually determined with the aid of simple energy loss calculations. As suggested by Fischella et al. [36], this approximation is not absolutely correct. Thus, instead of average proton beam energy ($\langle E \rangle$), effective proton beam energy (E_{eff}) of the Ni foil was estimated based on the relation suggested by Fischella et al. [36]. The calculated effective proton beam energies of the four Ni foils are 19.02 ± 0.76, 15.82 ± 0.86, 11.97 ± 1.03 and 7.25 ± 1.39 MeV, respectively. Then the corresponding activation cross section for the $^{\text{nat}}\text{Ni}(p,x)^{61}\text{Cu}$ reactions at the i-th sample, $\sigma(E_i)$ was determined by using the standard activation formula [37].

$$\sigma(E_i) = \frac{C(E_i).M}{N_a.\rho.t_h.\Phi.\varepsilon(E_\gamma).I_\gamma.f} \tag{7}$$

In order to avoid the direct measurement of proton beam intensity, Φ the cross section of $^{\text{nat}}\text{Ni}(p,x)^{61}\text{Cu}$ reaction has been determined using a known monitor reference cross section σ_r as well as from the activity of the copper foil, by the following equation:

$$\sigma_s(E_p) = \sigma_r \frac{C_s.M_s.N_a.\rho_r.t_{hr}.\varepsilon_r.I_{\gamma r}.f_r}{C_r.M_r.N_a.\rho_s.t_{hs}.\varepsilon_s.I_{\gamma s}.f_s} \tag{8}$$

where σ_r is the reference monitor cross-section taken from the $^{\text{nat}}\text{Cu}(p,x)^{62}\text{Zn}$ monitor reaction [25] recommended by IAEA. λ is the decay constant (s^{-1}) related to half live $T_{1/2}$ ($\lambda = \frac{\ln 2}{T_{1/2}}$) of the reaction product of interest. C_s and C_r are the net counts of the characteristic gamma lines of ^{61}Cu and ^{62}Zn respectively. The symbol $I_{\gamma s}$, $I_{\gamma r}$, are the branching intensities and ε_s, ε_r are the efficiencies of the γ-lines of ^{61}Cu and ^{62}Zn, respectively, N_a is the Avogadro's number (6.023×10^{23}), ρ_s and ρ_r are the target material densities, M_s and M_r are the atomic weight of the target material of nickel and copper while t_{hs} and t_{hr} are the target thickness (cm). The time factor, f_s and f_r are defined by

$$f_x = \left(1 - e^{-\lambda_x t_i}\right) e^{-\lambda_x t_{c,x}} \left(1 - e^{-\lambda_x t_{m,x}}\right) / \lambda_x \tag{9}$$

where t_i, t_c, t_m are the irradiation, cooling and counting time (s), respectively and $x = {}^{61}\text{Cu}$ or ^{62}Zn. The decay data such as the half-life $T_{1/2}$ and γ-ray emission probability (I_γ) in Eq. (8) as well as the γ-ray energy (E_γ) used in the detection efficiency were taken from the ENSDF evaluation [38,39] retrieved via the interface of Live Chart of nuclides [40] and summarized in Table 3. The Q-values and the threshold energies were accessed through the Q-tool system [41] and are presented along in Table 3.

3.3. Uncertainty in cross section measurement

The activation cross section for the reaction $^{\text{nat}}\text{Ni}(p,x)^{61}\text{Cu}$, $\sigma(E_i)$ was determined by considering only the dominant γ-line of 282.96 keV (12.2%). It was measured relative to the $^{\text{nat}}\text{Cu}(p,x)^{62}\text{Zn}$ monitor reaction cross section by measuring the activity of ^{62}Zn considering only the γ-line of 596.56 keV (26.0%). As seen from Eq. (8), the attributes observed with errors

Table 3
Decay data for the assessed radio-nuclides extracted from the interface of Live Chart of nuclides of IAEA [39] as well as Q-values and threshold energies extracted from Q-tool [40]. Bold γ-lines were used in derivation of experimental cross section in the present work.

Nuclide	Half-life (h)	Decay-mode	γ-Ray energy, E_γ (keV)	γ-Ray intensity, I_γ (%)	Contributing reaction	Q-value (MeV)	Threshold energy, Eth (MeV)
^{61}Cu	3.339 ± 0.008	EC + β^+ (100%)	**282.96**	**12.2 ± 2.2**	^{61}Ni$(p,n)^{61}$Cu	−3.02	3.07
					^{62}Ni$(p,2n)^{61}$Cu	−13.62	13.84
			656.01	10.8 ± 2.0			
^{62}Zn	9.193 ± 0.015	EC + β^+ (100%)	**596.56**	**26.0 ± 2.0**	^{63}Cu$(p,2n)^{62}$Zn	−13.26	13.48

in the present measurements are counts (C_s, C_r), atomic weight (M_s and M_r), γ-ray intensity ($I_{\gamma s}$, $I_{\gamma r}$), efficiency (ε_s, ε_r) and the time factor (f_s, f_r) related to decay constant λ. Due to lack of uncertainty information for the quantities; thickness (t_h) and target material density ρ, they have not been considered in the uncertainty analysis. The IAEA recommended charged-particles monitor reactions library [25] consisting of evaluated cross section data, believed to be accurate enough to meet the demand of all current applications [42]. Due to the lack of uncertainty information from the recommended library, σ_r is not considered in the uncertainty propagation of cross section. The uncertainty in the cross-section of each of the sample for the i-th measurement, is propagated as,

$$\left((\Delta\sigma_s)_i\right)^2 = \sum_s \left(\frac{\Delta(x_s)_i}{(x_s)_i}(\sigma_s)_i\right)^2 + \sum_r \left(\frac{\Delta(x_r)_i}{(x_r)_i}(\sigma_s)_i\right)^2 + 2\left(\frac{\Delta(\varepsilon_s)_i}{(\varepsilon_s)_i}(\sigma_s)_i\right) \times cor\left((\varepsilon_s)_i, (\varepsilon_r)_i\right)\left(\frac{\Delta(\varepsilon_r)_i}{(\varepsilon_r)_i}(\sigma_s)_i\right) \quad 1 \le s, r \le 5;\ 1 \le i \le 4; \tag{10}$$

where x_s and x_r denotes the attributes counts, atomic weight, γ-ray intensity, efficiencies and the time factors for the sample and monitor, respectively. Details of Eq. (10) are provided in Appendix. The covariance information related to the four measured cross sections of ^{nat}Ni$(p,x)^{61}$Cu is given in a 4 × 4 covariance matrix $V_{\sigma s}$, which is obtained by using the information on the partial uncertainties and the correlations between them, using the following relation,

$$(V_{\sigma_s})_{ij} = \sum_{kl} (e_k)_i (S_{kl})_{ij} (e_l)_j, \quad 1 \le i, j \le 4,\ 1 \le k, l \le 10 \tag{11}$$

where, $(e_k)_i = \frac{\partial(\sigma_s)_i}{\partial(x_k)_i}\Delta(x_k)_i$ is the partial uncertainty in $(\sigma_s)_i$ due to the kth attribute in the ith experimental observation and $(e_l)_j = \frac{\partial(\sigma_s)_j}{\partial(x_l)_j}\Delta(x_l)_j$ is the partial uncertainty in $(\sigma_s)_j$ due to the lth attribute in the jth experimental observation [33,43]. $(S_{kl})_{ij}$ represents the correlation between the kth attribute in the ith experimental observation and lth attribute in the jth experimental observation and called micro-correlation. Since the parameters t_i, t_c and t_m have been measured without uncertainties in the present experimental work, thus the only attribute that contributes to the uncertainty in the time factor, f is the decay constant, λ. The uncertainties in the time factors was propagated from the uncertainties in the decay constants [24], given by

$$(\Delta f/f)^2 = s_{f\lambda}^2 (\Delta\lambda/\lambda)^2 \tag{12}$$

Table 4
Partial uncertainty in various attributes and their corresponding correlation to obtain the $^{nat}Ni(p,x)^{61}Cu$ reaction cross-section.

Attributes	Partial uncertainties in $^{nat}Ni(p,x)^{61}Cu$ reaction cross-section				Correlation
	$E_p = 19.02$ (MeV)	$E_p = 15.82$ (MeV)	$E_p = 12.12$ (MeV)	$E_p = 7.45$ (MeV)	
γ-Ray peak Counts, C_{Cu}	0.160	0.123	0.069	0.087	0
γ-Ray intensity, $I_{\gamma Cu}$	1.951	1.089	0.328	0.742	1
Efficiency of the detector, ε_{Cu} [a]	0.487	0.272	0.082	0.185	1
Time factor, f_{Cu}	0.020	0.011	0.003	0.007	1
Atomic weight, M_{Cu}	3.687E−05	2.058E−05	6.193E−06	1.402E−05	1
γ-Ray peak Counts, C_{Zn}	0.149	0.083	0.025	0.057	1
γ-Ray intensity, $I_{\gamma Zn}$	0.832	0.465	0.140	0.316	1
Efficiency of the detector, ε_{Zn} [a]	0.498	0.278	0.084	0.189	1
Time factor, f_{Zn}	0.015	0.009	0.003	0.006	1
Atomic weight, M_{Zn}	5.108E−04	2.851E−04	8.580E−05	1.942E−04	1

Correlation within the attributes 0 represents uncorrelated and 1 for fully correlated.
[a] Partially correlated with correlation 0.86 [Table 2].

$f = f_s$ or f_r and $\lambda = \lambda_s$ or λ_r with relative sensitivity $s_{f\lambda}$

$$s_{f\lambda} = \frac{\lambda}{f}\frac{\partial f}{\partial \lambda} = \left(\frac{\lambda t_i e^{-\lambda t_i}}{1 - e^{-\lambda t_i}} - \lambda t_c + \frac{\lambda t_m e^{-\lambda t_m}}{1 - e^{-\lambda t_m}} - 1\right) \tag{13}$$

The uncertainty in decay constant, $\Delta\lambda = (\ln 2 \Delta T_{1/2})/T_{1/2}^2$ where $T_{1/2}$ and $\Delta T_{1/2}$ was taken from the ENSDF evaluation extracted from the interface of Live Chart of Nuclides of IAEA [38–40]. The partial uncertainties due to the various attributes involved in the cross section measurement of $^{nat}Ni(p,x)^{61}Cu$ reaction relative to $^{nat}Cu(p,x)^{62}Zn$ monitor reaction are summarized in Table 4. The attribute C_s in all the measurements are uncorrelated and therefore the corresponding micro-correlation matrix is an identity matrix. The observations of γ-ray intensity $I_{\gamma s}$, $I_{\gamma r}$ with reference to same characteristic γ-rays are identical and hence they are fully correlated in all four measurements, but the observations with reference to different characteristic γ-rays are independent and not correlated. Similarly, the micro-correlation associated with the pair of attributes (M_s, M_r) and the time factor (f_s, f_r) are independent hence not correlated, but observations of same attribute used in four different measurements are fully correlated (same atomic weight and half-life of nuclide used in all four measurement). The micro-correlation of ε_s and ε_r with reference to the same characteristic γ-lines are fully correlated. However, there exist a partial correlation between ε_s and ε_r since same efficiency interpolation model was used and the partial correlation coefficients were taken from Table 2. The final covariance in the cross-section was constructed by substituting the partial uncertainties data and the corresponding micro-correlation in Eq. (11).

4. Theoretical calculation of cross-section using nuclear model

For a better understanding of the experimental data, it is instructive and advantageous to perform theoretical calculation of cross-sections using nuclear model and compare the experimental values with the calculated data. The measured $^{nat}Ni(p,x)^{61}Cu$ reaction cross-section have been calculated theoretically using nuclear model code TALYS 1.8 [26] up to a proton energy of 60 MeV. TALYS is a software for the analysis and prediction of nuclear reactions that involve

neutrons, photons, protons, deuterons, tritons, ^{3}He and alpha particles, in the 1 keV to 200 MeV energy range and for target nuclides of mass 5 and heavier [44]. Theoretical calculations of nuclear reaction cross-sections include the direct interaction, pre-equilibrium and compound nucleus contributions. To calculate the cross-sections using the compound nucleus model as well as the pre-equilibrium models, one of the most important ingredients is the level density, it is an important characteristic of the nucleus, as it allows one to explore the mechanism of nuclear excitations, information about the structure of the excited nuclei. A correct level density is the most crucial ingredient for a reliable theoretical analysis of cross sections, spectra, angular distributions, and other nuclear reaction observables. In view of this, in the present work the nuclear level densities calculations of the nuclei were performed using both the Generalised superfluid model (GSM) and Back-shifted Fermi gas model (BFM) available from TALYS [26]. For the theoretical calculations with Generalised superfluid model (GSM), no parameters were adjusted. However, for theoretical calculation using the Back-shifted Fermi gas model the energy-dependent level density parameter a, has been adopted, which takes into account the damping of shell effects and is given by

$$a = a(E_x) = \tilde{a}\left[1 + \delta W \frac{1 - e^{-\gamma U}}{U}\right] \tag{14}$$

where U is the excitation energy, δW is the shell correction energy, and γ is the shell damping parameter The asymptotic level density parameter $\tilde{a}$ is of the form

$$\tilde{a} = \alpha A + \beta A^{2/3} \tag{15}$$

The shell damping factor, γ depends on the mass number A and is given by $\frac{\gamma_1}{A^{1/3}} + \gamma_2$, where γ_1 and γ_2 are global parameters that have been determined to give the best average level density description over a whole range of nuclides. Also the γ-ray strength function has also been studied using the Brink–Axel Lorentzian, available from TALYS 1.8. The pre equilibrium contribution was calculated by two component excitation model. The excitation model for pre-equilibrium nuclear reactions has proven to be powerful for the analysis of continuum emission spectra and excitation functions for projectile energies above several MeV. Pre-equilibrium emission takes place after the first stage of the reaction but long before statistical equilibrium of the compound nucleus is attained, leading to the well-known high-energy tails in the emission spectra and the smooth forward peaked angular distributions [45]. Gamma-ray transmission coefficients are important for the description of the gamma-ray emission channel in nuclear reactions. Hence the theoretical calculations have been performed with the Generalised superfluid model (GSM) with other parameter values taken as default but for nuclear level densities calculations with Back-shifted Fermi gas model (BFM), the level-density parameters; α, β, γ_1 as well as the γ-ray strength function was adjusted. The $^{\text{nat}}$Ni$(p, x)^{61}$Cu reaction cross section theoretically calculated from the nuclear model code TALYS 1.8 is plotted in Fig. 4.

5. Results and discussions

The experimentally determined $^{\text{nat}}$Ni$(p, x)^{61}$Cu reaction cross-sections along with their uncertainties at different proton beam energies are reported in Table 5. The effective proton beam energy and its uncertainty are due to the beam energy distribution in the stack, which is elaborately discussed by Fisichella et al. [36]. This is because the beam energy degrades as it traverses the different stack foil due to energy straggling and foil thickness. Hence from the beam energy distribution in the stack targets, the energy and its uncertainty is obtained. As mentioned by

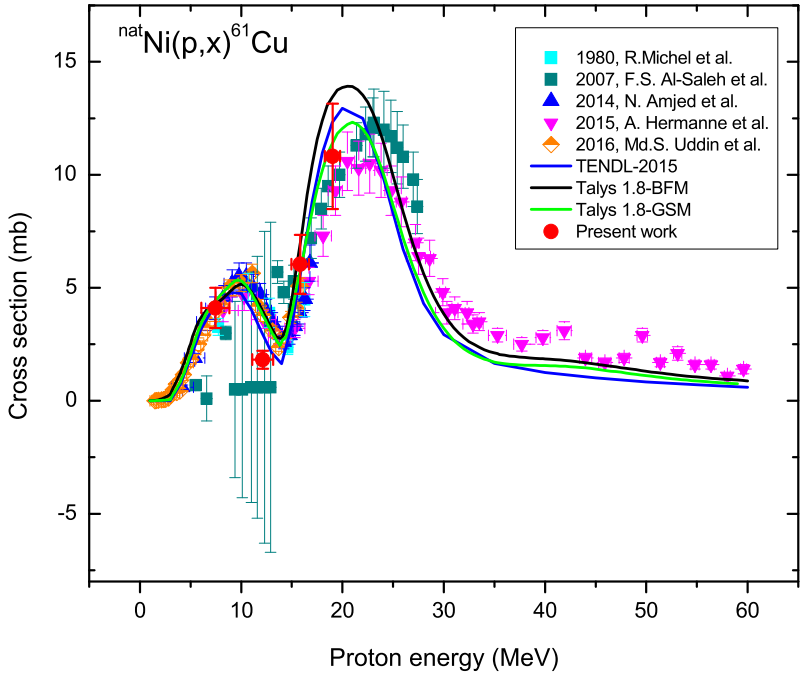

Fig. 4. The excitation function of the ^{nat}Ni$(p, x)^{61}$Cu reaction cross sections with literature data and the calculated values from TALYS-1.8 along with the evaluated data of TENDL-2015.

Table 5
The experimentally determined ^{nat}Ni$(p, x)^{61}$Cu reaction cross section (σ_s) along with its uncertainty.

Proton energy, E_p (MeV)		^{nat}Ni$(p, x)^{61}$Cu reaction cross section, σ_s (mb)	Correlation matrix			
Average energy Ref. [35]	Effective energy Ref. [36]					
18.89 ± 0.76	19.02 ± 0.76	10.82 ± 2.34	1.00			
15.70 ± 0.86	15.82 ± 0.86	6.04 ± 1.31	0.99	1.00		
11.97 ± 1.03	12.12 ± 1.03	1.82 ± 0.40	0.98	0.98	1.00	
7.25 ± 1.39	7.45 ± 1.39	4.11 ± 0.89	0.99	0.99	0.98	1.00

Fisichella et al. [36], to which exact proton energy the cross section should be attributed. Thus we have done the in and out proton energy calculation by using the SRIM 2013 code of Ziegler [35] to obtained the average proton beam energy as mentioned before. We have also calculated the effective proton beam energy using the prescription of Fisichella et al. [36], which has also been mentioned before. Thus we have assigned the reaction cross section to the effective proton beam energy. For the proton flux calculation also we have used the monitor reaction cross section corresponding to the effective proton beam energy faced by the monitor foil owing to the energy loss in the different layers. In fact, it is true that the effective proton energies of Ni target foils and Cu monitor foils are not same. However, we have assumed that the proton flux practically remains same for all the foils. We have also used monitor reaction cross section without uncertainty. This is because in the reaction monitor cross section, no uncertainty is given in ref. [25] recommended by IAEA. All these factors can affect the uncertainty of reaction cross section. Using covariance analysis the total uncertainty in the cross section was determined to be 21.58, 21.63, 21.86 and

21.63% at effective proton energies of 19.02, 15.82, 12.12 and 7.45 MeV, respectively. The high uncertainty in the cross-section was due to the major contribution of uncertainty from γ-ray intensities of both the monitor and the sample with an uncertainty of 7–18%. The uncertainty due to the use of effective proton beam energy will be within the mentioned uncertainty limit. Thus the $^{nat}Ni(p,x)^{61}Cu$ reaction cross sections given in Table 5 are for the effective proton beam energy with mentioned uncertainty.

The present data is compared with existing literature data of N. Amjed et al. [1], R. Michel et al. [18], F.S. Al Saleh et al. [19], Hermanne et al. [20], and Md.S. Uddin et al. [21] retrieved from IAEA-EXFOR database [22,23] and plotted as a function of proton energy in Fig. 4. The $^{nat}Ni(p,x)^{61}Cu$ reaction cross sections from the present work plotted in Fig. 4 are also have the uncertainty limit of effective proton energy. It is seen from Fig. 4 that the present datum at 7.45 MeV is in excellent agreement with the data of N. Amjed et al. [1] and the data of Md.S. Uddin et al. [21]. However, the datum at 12.12 MeV is low in comparison to the data of N. Amjed et al. [1], Hermanne et al. [20] and Md.S. Uddin et al. [21]. At the proton energies of 15.82 and 19.02 MeV, the present data are in close agreement to the experimental data of N. Amjed et al. [1], F.S. Al Saleh [19] and Hermanne et al. [20] within uncertainty limit. The experimentally determined $^{nat}Ni(p,x)^{61}Cu$ reaction cross sections were further compared with the TALYS based TENDL-2015 data library [46] which are also plotted in Fig. 4. It can be seen that the weighted average values obtained from TENDL-2015 library are in excellent agreement with the present data at the proton energies of 7.45 MeV and 15.82 MeV but it is slightly higher at 19.02 MeV and relatively high at 12.12 MeV. Similarly, TENDL-2015 values are comparatively higher than literature data between 16–24 MeV but lower than experimental data of Hermanne et al. [20] above the proton energy of 25 MeV.

The theoretical values from computer code TALYS-1.8 [26] was calculated by varying only the level density using the Generalised superfluid model (GSM) available from TALYS, which are also plotted along in Fig. 4 for comparison. The theoretical values calculated using GSM for the level density follows similar trend with TENDl-2015 agreeing with literature data of N. Amjed et al. [1], R. Michel et al. [18], Hermanne et al. [20], and Md.S. Uddin et al. [21] between 3–15 MeV and it is higher at proton energies of 16–24 MeV. The Generalised superfluid model (GSM) well predicted the present result at proton energies of 7.45, 15.82 and 19.02 MeV but it do not at all agree with the present datum at 12.12 MeV and with the measured data of Hermanne et al. [20] above the proton energy of 25 MeV as it is relatively low. Further the excitation function of the $^{nat}Ni(p,x)^{61}Cu$ reaction as a function of proton energy from 3 to 60 MeV have been calculated by using the Back-shifted Fermi gas model (BFM) with adjusted parameters along with the γ-ray strength function of Brink–Axel Lorentzian in order to further examine the discrepancies between the literature data and TENDL-2015 as well as to check the reliability of the present measurement. The resulting theoretically calculation values are plotted in Fig. 4 for comparison. It is seen the present data at the proton energies of 7.45 and 15.82 MeV are in good agreement with the theoretical values calculated using BFM. Also the theoretically calculated cross section of $^{nat}Ni(p,x)^{61}Cu$ using BFM agrees well with all the experimental data of R. Michel et al. [18], N. Amjed et al. [1], Hermanne et al. [20] and Md.S. Uddin et al. [21] at the proton energies of 3–15 MeV and with the data of Hermanne et al. [20] between 25–31 MeV and 45–60 MeV but it is comparatively high at the energies between 16–24 MeV following the same trend with that of the GSM model and TENDL-2015. The present experimental cross-sections of the $^{nat}Ni(p,x)^{61}Cu$ reaction along with the evaluated values from TENDL-2015 library and theoretically calculated value of TALYS 1.8 are summarized in Table 6. It can be seen that the experimental cross-sections of the $^{nat}Ni(p,x)^{61}Cu$ reaction at the proton energies of 7.45, 15.82

Table 6
The experimentally determined $^{nat}Ni(p,x)^{61}Cu$ reaction cross section (σ_s) along with TALYS-1.8 [26] and the evaluated cross sections from TENDL-2015 [45].

Proton energy, E_p (MeV)		$^{nat}Ni(p,x)^{61}Cu$ reaction cross section, σ_s (mb)			
Average energy Ref. [35]	Effective energy Ref. [36]	Present work	Talys 1.8-GSM	Talys 1.8-BFM	Tendl-2015
18.89 ± 0.76	19.02 ± 0.76	10.82 ± 2.34	11.38	13.43	12.17
15.70 ± 0.86	15.82 ± 0.86	6.04 ± 1.31	5.72	6.08	5.22
11.97 ± 1.03	12.12 ± 1.03	1.82 ± 0.40	3.94	4.09	3.09
7.25 ± 1.39	7.45 ± 1.39	4.11 ± 0.89	4.28	4.23	4.06

and 19.02 MeV are in close agreement with the values from TENDL-2015 library [46] as well as with the value based on TALYS-1.8 [26] within uncertainty limit but the present datum at 12.12 MeV is very low when compared with data from TENDL-2015 library and TALYS-1.8.

The above discussion indicates that the agreement or disagreement of present and literature data with the values from TENDL-2015 library [46] and theoretical values from TALYS-1.8 [26] depends on the various parameters in the theoretical models. On the other hand, measurements of experimental values by stack-foil activation technique depends on the degradation of the beam quality due to the statistical nature of energy loss processes as it passes through the non-uniform stack targets [36]. This can affects in the reaction cross section and causes disagreement among the literature data.

6. Conclusion

The $^{nat}Ni(p,x)^{61}Cu$ reaction cross sections at the effective proton beam energies of 7.45, 12.12, 15.82 and 19.02 MeV relative to the $^{nat}Cu(p,x)^{62}Zn$ monitor reaction were measured and covariance analysis has been carried out to determine the uncertainty. The present data at the effective proton beam energies of 7.45, 15.82 and 19.02 MeV are in good agreement with the literature data. The excitation function of the $^{nat}Ni(p,x)^{61}Cu$ reaction as a function of proton energy from 3 to 60 MeV have been calculated theoretically by using the computer code TALYS-1.8. The values from TALYS-1.8 well predicted the present data at the effective proton beam energies of 7.45, 15.82 and 19.02 MeV and earlier data between 3–15 MeV and 25–31 MeV. It also follows a similar trend with the values of TENDL-2015 library. However, values from both TALYS-1.8 and TENDL-2015 library are higher than the literature data between 16–24 MeV. Therefore the present data are useful to increase the reliability and enrich the database for the production of medical radioisotope ^{61}Cu. The detailed description of the uncertainties and covariance analysis ensures that the experimental results can be incorporated in the evaluation process.

Acknowledgements

The authors are thankful to the staffs of Tata Institute of Fundamental Research (TIFR), Mumbai for their excellent operation of the accelerator and for providing the proton beam for our experiment. One of the authors (S. Badwar) expresses her sincere gratitude to the Board of Research in Nuclear Sciences, Department of Atomic Energy, Mumbai for funding the research project. She is also grateful to Tim Vidmar, SCK CEN, Belgian Nuclear Research Centre, Boeretang 200, BE-2400 Mol, Belgium, for providing the EFFTRAN code.

Appendix A. Determination of cross section

The activity cross section as given in Eq. (8)

$$\sigma_s(E_p) = \sigma_r \frac{C_s.M_s.N_a.\rho_r.t_{hr}.\varepsilon_r.I_{\gamma r}.f_r}{C_r.M_r.N_a.\rho_s.t_{hs}.\varepsilon_s.I_{\gamma s}.f_s} \tag{A.1}$$

The sources of uncertainty in the cross-section calculation are C, M, I_γ, ε and f related to both the sample and the monitor. However, the reference cross section σ_r is treated as a constant in the uncertainty propagation of cross section due to lack of uncertainty information of the quantity from the recommended database. Therefore there are ten attributes contributing to the uncertainty propagation of cross section. Hence, σ_s can be treated as a function of C, M, I_γ, ε and f of both the sample and monitor and can be expressed as,

$$\sigma_s = f(C, M, \varepsilon, I_\gamma, f) \tag{A.2}$$

Considering Taylor series expansion of Eq. (A.2) and ignoring higher order terms, assuming that the uncertainty is small, the uncertainty in cross section can be propagated as

$$\begin{aligned}(\Delta\sigma_s)^2 = &\sum_s \left(\frac{\partial\sigma_s}{\partial x_s}\Delta x_s\right)^2 + \sum_r \left(\frac{\partial\sigma_s}{\partial x_r}\Delta x_r\right)^2 \\ &+ 2\sum_{sr}\left(\frac{\partial\sigma_s}{\partial x_s}\Delta x_s\right) cor(x_s, x_r)\left(\frac{\partial\sigma_s}{\partial x_r}\Delta x_r\right), \quad 1 \le s, r \le 5\end{aligned} \tag{A.3}$$

Among all the physical quantities used in cross section calculation except for the efficiencies, the observations between any two other pair of attributes (e.g. (Cs, Cr), (Cs, $I_\gamma s$) and so on) are independent of each other hence no correlation exist between them. However, a partial correlation exists only between the efficiencies attribute of sample and monitor ε_s and ε_r because of the same detector model which was used in the efficiency interpolation to obtain the efficiency of both the sample and monitor. Therefore Eq. (A.3) reduces to

$$\begin{aligned}(\Delta\sigma_s)^2 = &\sum_s \left(\frac{\partial\sigma_s}{\partial x_s}\Delta x_s\right)^2 + \sum_r \left(\frac{\partial\sigma_s}{\partial x_r}\Delta x_r\right)^2 \\ &+ 2\left(\frac{\partial\sigma_s}{\partial\varepsilon_s}\Delta\varepsilon_s\right) cor(\varepsilon_s, \varepsilon_r)\left(\frac{\partial\sigma_s}{\partial\varepsilon_r}\Delta\varepsilon_r\right), \quad 1 \le s, r \le 5\end{aligned} \tag{A.4}$$

The partial uncertainty in the cross section measurement due to the kth attribute is given as

$$\frac{\partial\sigma_s}{\partial x_k}\Delta x_k = \frac{\Delta x_k}{x_k}\sigma_s \tag{A.5}$$

which is obtain by considering the rest of the other attributes as constant. Hence Eq. (A.4) can be rewritten as

$$\begin{aligned}(\Delta\sigma_s)^2 = &\left(\frac{\Delta C_s}{C_s}\sigma_s\right)^2 + \left(\frac{\Delta M_s}{M_s}\sigma_s\right)^2 + \left(\frac{\Delta\varepsilon_s}{\varepsilon_s}\sigma_s\right)^2 + \left(\frac{\Delta I_{\gamma s}}{I_{\gamma s}}\sigma_s\right)^2 + \left(\frac{\Delta f_s}{f_s}\sigma_s\right)^2 \\ &+ \left(\frac{\Delta C_r}{C_r}\sigma_s\right)^2 + \left(\frac{\Delta M_r}{M_r}\sigma_s\right)^2 + \left(\frac{\Delta\varepsilon_r}{\varepsilon_r}\sigma_s\right)^2 + \left(\frac{\Delta I_{\gamma r}}{I_{\gamma r}}\sigma_s\right)^2 + \left(\frac{\Delta f_r}{f_r}\sigma_s\right)^2 \\ &+ 2\left(\frac{\Delta\varepsilon_s}{\varepsilon_s}\sigma_s\right) cor(\varepsilon_s, \varepsilon_r)\left(\frac{\Delta\varepsilon_r}{\varepsilon_r}\sigma_s\right)\end{aligned} \tag{A.6}$$

References

[1] N. Amjed, F. Tárkányi, A. Hermanne, F. Ditrói, S. Takács, M. Hussain, App. Radiat. Isot. 92 (2014) 73.
[2] A. Hermanne, S. Takács, R. Adam-Rebeles, F. Tárkányi, M.P. Takács, Nucl. Instrum. Methods B 299 (2013) 8.
[3] U. Fisher, IFMIF deuteron and proton data needs, https://www-nds.iaea.org/fendl30/about/fischer-2.pdf, 2009 (Accessed 13 January 2015).
[4] K. Ammon, I. Leya, B. Lavielle, E. Gilabert, J.-C. David, U. Herpers, R. Michel, Nucl. Instrum. Methods B 266 (2008) 2.
[5] A.R. Usman, M.U. Khandaker, H. Haba, M. Murakami, N. Otuka, Nucl. Instrum. Methods B 368 (2016) 112.
[6] R. Strangis, C.G. Lepera, Cyclotrons and their applications, in: Eighteenth International Conference, 2007.
[7] F. Szelecsenyi, G. Blessing, S.M. Qaim, App. Radiat. Isot. 44 (1993) 575.
[8] D.W. McCarthy, L.A. Bass, P.D. Cutler, R.E. Shefer, R.E. Klinkowstein, P. Herrero, J.S. Lewis, C.S. Cutler, C.J. Anderson, M.J. Welch, Nucl. Med. & Biol 26 (1999) 351.
[9] P. Rowshanfarzada, M. Sabet, A.R. Jalilian, M. Kamalidehghan, Appl. Radiat. Isot. 64 (2006) 1563.
[10] H. Muramatsu, E. Shirai, H. Nakahara, Y. Murakami, Appl. Radiat. Isot. 29 (1978) 611.
[11] L.A. Bass, D.W. McCarthy, L.A. Jones, P.D. Cutler, R.E. Shefer, R.E. Klinkowstein, S.W. Schwarz, C.S. Cutler, J.S. Lewis, C.J. Anderson, M.J. Welch, J. Label. Compd. Radiopharm. 40 (1997) 325.
[12] V. Tolmachev, H. Lundqvist, L. Einarsson, Appl. Radiat. Isot. 49 (1998) 79.
[13] T. Fukumura, K. Okada, F. Szelecsenyi, Z. Kovacs, K. Suzuki, Radiochim. Acta 92 (2004) 209.
[14] M.N. Aslam, S.M. Qaim, Appl. Radiat. Isot. 89 (2014) 65.
[15] B.P. Singh, M.K. Sharma, M.M. Musthafa, H.D. Bhardwaj, R. Prasad, Nucl. Instrum. Methods A 562 (2006) 717.
[16] S. Thieme, M. Walther, S. Preusche, J. Rajander, H.J. Pietzsch, J.O. Lill, M. Kaden, O. Solin, J. Steinbach, Appl. Radiat. Isot. 72 (2013) 169.
[17] E. Garrido, C. Duchemin, A. Guertin, F. Haddad, N. Michel, V. Métivier, Nucl. Instrum. Methods B 383 (2016) 191.
[18] R. Michel, G. Brinkmann, J. Radioanal. Chem. 59 (1980) 467.
[19] F.S. Al Saleh, K.S. Al Mugren, A. Azzam, Appl. Radiat. Isot. 65 (2007) 104.
[20] A. Hermanne, R. Adam Rebeles, F. Tarkanyi, S. Takacs, Nucl. Instrum. Methods B 345 (2015) 58.
[21] Md.S. Uddin, A.K. Chakraborty, S. Spellerberg, Md.A. Shariff, S. Das, Md.A. Rashid, I. Spahn, S.M. Qaim, Radiochim. Acta 104 (2016) 305.
[22] IAEA–EXFOR experimental nuclear reaction data base, available at http://www-nds.iaea.org/exfor.
[23] N. Otuka, E. Dupont, V. Semkova, B. Pritychenko, A.I. Blokhin, M. Aikawa, S. Babykina, M. Bossant, G. Chen, S. Dunaeva, R.A. Forrest, T. Fukahori, N. Furutachi, S. Ganesan, Z. Ge, O.O. Gritzay, M. Herman, S. Hlavač, K. Katō, B. Lalremruata, Y.O. Lee, A. Makinaga, K. Matsumoto, M. Mikhaylyukova, G. Pikulina, V.G. Pronyaev, A. Saxena, O. Schwerer, S.P. Simakov, N. Soppera, R. Suzuki, S. Takács, X. Tao, S. Taova, F. Tárkányi, V.V. Varlamov, J. Wang, S.C. Yang, V. Zerkin, Y. Zhuang, Nucl. Data Sheets 120 (2014) 272.
[24] N. Otsuka, B. Lalremruata, M.U. Khandaker, A.R. Usman, L.R.M. Punte, Radiat. Phys. Chem. 140 (2017) 502.
[25] S.M. Qaim, F. Tárkányi, P. Obložinskỳ, K. Gul, A. Hermanne, M.G. Mustafa, F.M. Nortier, B. Scholten, Yu. Shubin, S. Takács, Y. Zhuang, Charged particle cross-section database for medical radioisotope production: diagnostic radioisotopes and monitor reactions, Vienna, IAEA-TECDOC-1211, data updated in January 2007, available at http://www-nds.iaea.org/medical/monitor_reactions.html.
[26] A.J. Koning, S. Hilaire, S. Goriely, TALYS User Manual: A Nuclear Reaction Program, NRG-1755, ZG PETTEN, The Netherlands, 2015.
[27] M. Berglund, M.E. Wieser, Isotopic compositions of the elements 2009 (IUPAC Tech. Report), Pure Appl. Chem. 83 (2011) 397–410.
[28] M.J. Martin, Nucl. Data Sheets 114 (2013) 1497.
[29] National Nuclear Data Center, Brookhaven National Laboratory, http://www.nndc.bnl.gov/.
[30] T. Vidmar, Nucl. Instrum. Methods Phys. Res., Sect. A 550 (2005) 603.
[31] L.P. Geraldo, D.L. Smith, Nucl. Instrum. Methods Phys. Res, Sect. A 290 (1990) 499.
[32] Y. Santhi Sheela, H. Naik, K. Manjunatha Prasad, S. Ganesan, N.S. Nair, S.V. Suryanarayana Tech, Rep. No. MU/STATISTICS/DAE-BRNS/2017/1, available online https://www.researchgate.net/publications/31384207.
[33] R. Ghosh, S. Badwar, B. Lawriniang, Y.S. Sheela, H. Naik, Y. Naik, S.V. Suryanarayana, B. Jyrwa, S. Ganesan, J. Radioanal. Nucl. Chem. 314 (2017) 1983.
[34] R. Ghosh, B. Lawriniang, S. Badwar, S.S. Yerraguntla, H. Naik, B.J. Patil, Y. Naik, S.V. Suryanarayana, B. Jyrwa, S. Ganesan, https://doi.org/10.1515/ract-2017-2855.
[35] J.F. Ziegler, SRIM-2013, Nucl. Instrum. Methods B 219 (2004) 1027, http://www.srim.org/.

[36] M. Fisichella, A.C. Shotter, A. Di Pietro, P. Figuera, M. Lattuada, C. Marchetta, V. Privitera, L. Romano, C. Ruiz, M. Zadro, Phys. Rev. C 92 (2015) 064611.
[37] K. Kim, M.U. Kandaker, H. Naik, G. Kim, Nucl. Instrum. Methods B 322 (2014) 63.
[38] A.L. Nichols, B. Singh, J.K. Tuli, Nucl. Data Sheets 113 (2012) 973.
[39] K. Zuber, B. Singh, Nucl. Data Sheets 125 (2015) 1.
[40] IAEA, Live Chart of Nuclides, Interactive Chart of Nuclides, International Atomic Energy, 2009, available at https://www-nds.iaea.org/.
[41] Qtool, Calculation of Reaction Q-Values and Thresholds, Los Alamos National Laboratory, T-2 Nuclear Information Service, available from http://t2.lanl.gov/nis/data/qtool.html.
[42] A. Hermanne, A.V. Ignatyuk, R. Capote, B.V. Carlson, J.W. Engle, M.A. Kellet, T. Kibedi, G. Kim, F.G. Kondev, M. Hussain, O. Lebeda, A. Luca, Y. Nagai, H. Naik, A.L. Nichols, F.M. Nortier, S.V. Suryanarayana, S. Takács, F.T. Tárkányi, M. Verpelli, Nucl. Data Sheets 148 (2018) 338.
[43] S.S. Yerraguntla, H. Naik, M.P. Karantha, S. Ganesan, S.V. Suryanarayana, S. Badwar, J. Radioanal. Nucl. Chem. 314 (2017) 457, https://doi.org/10.1007/s10967-017-5374(2017).
[44] A.J. Koning, D. Rochman, Nuclear Research and Consultancy Group NRG, P.O. Box 25, 1755 ZG Petten, The Netherlands, 2012.
[45] A.J. Koning, M.C. Duijvestijn, Nucl. Phys. A 744 (2004) 15.
[46] A.J. Koning, D. Rochman, J. Kopecky, J.Ch. Sublet, M. Fleming, E. Bauge, S. Hilaire, P. Romain, B. Morillon, H. Duarte, S.C. van der Marck, S. Pomp, H. Sjostrand, R. Forrest, H. Henriksson, O. Cabellos, S. Goriely, J. Leppanen, H. Leeb, A. Plompen, R. Mills, https://tendl.web.psi.ch/tendl_2015.